# Reduced-Order Phase-Amplitude Characterization of Nonlinear Subsynchronous Oscillations Involving Inverter-Based Resources

Kaiyang Huang, *Student Member, IEEE,* Dan Wilson, Tianwei Xia, Kai Sun, *Fellow, IEEE*
*Department of Electrical Engineering and Computer Science, University of Tennessee*, Knoxville, TN
khuang12@vols.utk.edu, dwilso81@utk.edu, tianweixia@gmail.com, kaisun@utk.edu

2025 IEEE Power & Energy Society General Meeting (PESGM) | 979-8-3315-0995-8/25/$31.00 ©2025 IEEE | DOI: 10.1109/PESGM52009.2025.11225014

***Abstract*—This paper addresses the challenges associated with nonlinear Subsynchronous Oscillations (SSOs) induced by Inverter-Based Resources (IBRs) in power systems. Through adaptive isostable coordinate-based phase reduction, we introduce a 2-dimensional reduced model to analyze limit cycles in a two-area power system including one IBR. In particular, the methodology focuses on exploring nonlinear oscillations induced by Hopf bifurcation, providing insights into frequency-amplitude responses. The accuracy of the reduced-order model is verified by numerical studies compared with the full-order model. Our research contributes by presenting a novel model reduction technique and advancing the understanding of limit cycles in IBR-integrated power systems. This offers valuable implications for the stability and performance of modern power grids with increased IBR penetration.**

***Index Terms*—Inverter-based resource, subsynchronous oscillation, limit cycle, Hopf bifurcation, phase reduction, isostable coordinates, nonlinear oscillation.**

## I. Introduction

While penetrations of inverter-based resources (IBRs) are rapidly increasing globally, the usage of IBRs has brought about unwanted effects, including subsynchronous oscillations (SSOs) [1]. To address these issues, advanced solutions such as SSO adaptive damping controllers have been proposed for oscillations characterized by fixed points [2]. However, there is a need for a comprehensive understanding and mitigation strategy for various oscillatory phenomena, especially nonlinear oscillations induced by bifurcations. It is essential to note that if the oscillation is associated with a stable limit cycle, the oscillation becomes sustained, which has been observed in some SSO events. [3], [4].

In contrast to the effective analysis and control of linear oscillations using various tools designed for linear systems, the exploration of limit cycles poses challenges in high-dimensional dynamic systems. In addition, the frequency of a limit cycle cannot be fully characterized by the analysis of fixed points. This challenge can lead to confusion when observing undamped oscillations in reality without the corresponding identification of eigenpairs through eigenanalysis.

The growing complexity and high dimensionality of modern power systems pose significant challenges to their analysis and control. Full-order models, while comprehensive, are computationally expensive and often impractical for real-time nonlinear optimal control or detailed analytical studies such as time domain simulations [5]. For instance, understanding and characterizing nonlinear SSOs demands efficient methods that go beyond traditional linearization approaches. Reduced-order modeling, such as phase reduction [6], provides a transformative solution to these challenges by drastically simplifying the dimensionality of the system. By reducing a high-dimensional limit cycle oscillator to a one-dimensional ordinary differential equation, phase reduction captures the essential dynamics of the system in a more tractable form. This enables the development of optimal control strategies [7] and analytical insights that would be otherwise obscured in the full-order model.

However, this impressive reduction in dimensionality comes with the requirement that the magnitude of perturbations must be uniformly bounded in time by $\epsilon$, where $0 < \epsilon \ll 1$, to ensure the validity of the results to first-order accuracy in $\epsilon$. Considering this limitation of phase reduction, an alternative approach to broaden its applicability involves utilizing phase-amplitude coordinate systems. These systems account for transient dynamics in directions transverse to the periodic orbit. Recent advancement in this direction is the adaptive phase-amplitude reduction strategy in [8], [9], which incorporates the standard definition of asymptotic phase based on isochrons [10] and additionally considers slowly decaying isostable coordinates [11], representing level sets of the slowest decaying Koopman eigenfunctions [12]. By considering a family of limit cycles emerging for different parameter sets, the adaptive selection of the nominal parameter set helps limit errors in the reduced-order equations.

The paper presents several notable contributions. While there exist studies examining limit cycles induced by switching of controllers [3], [4], the literature on methodologies for model reduction of power system SSOs involving IBRs, remains limited. Addressing this gap, the paper introduces a novel reduced-order phase-amplitude model tailored for characterizing limit cycles in power systems. Initially, a nonlinear SSO is constructed and its source is explained and discussed. Through comprehensive case studies, the proposed model demonstrates great accuracy in capturing oscillatory dynamics while maintaining a low-dimensional representation. Further-

This work was supported by the National Science Foundation in part under grant ECCS-2329924 awarded to K. Sun, and in part under grant NSF-2140527 awarded to D. Wilson.

more, the frequency-amplitude characterization of the SSO is analyzed based on the reduced-order model. Comparative analysis between two reduced models further highlights the efficacy of the proposed approach. Notably, while the full-order model often suffers from the curse of dimensionality in designing control strategies, the implemented control strategy for both reduced-order models shows promising accuracy with significantly lower dimensions, which underscores the practical value of the proposed model in mitigating SSOs.

## II. Model Reduction

### A. Isochrons and Phase Reduction

Consider a dynamical system of the form:

$$\dot{\mathbf{x}} = \mathbf{f}\left(\mathbf{x}, p_0, \mathbf{u}\right), \tag{1}$$

where $\mathbf{x} \in \mathbb{R}^N$ denotes the state variable, $\mathbf{f} \in \mathbb{R}^N$ is the vector field describing system dynamics, $p_0 \in \mathbb{R}$ is some parameter, and $\mathbf{u} \in \mathbb{R}^M$ is an input from controllers. Suppose that (1) has a stable $T(p_0)$-periodic orbit solution $\mathbf{x}^\gamma_{p_0}$ for a constant choice of $p_0$ when $\mathbf{u} = \mathbf{0}$. A phase of nonlinear oscillation can be defined by $\theta \in [0, 2\pi)$ for all states $\mathbf{x} \in \mathbf{x}^\gamma_{p_0}$, with $\theta$ scaled so that $\dot{\theta} = 2\pi/T(p_0) = \omega(p_0)$ when $\mathbf{u} = \mathbf{0}$. Note that this definition builds a bijection mapping between $\theta$ and $\mathbf{x} \in \mathbf{x}^\gamma_{p_0}$. The definition of phase can be extended to the whole basin of attraction $\mathcal{D}_{p_0}$ of $\mathbf{x}^\gamma_{p_0}$ by isochrons [6]. For instance, let $\theta_1$ be the phase associated with some $\mathbf{a} \in x^\gamma_{p_0}$, the $\theta_1$ isochron is defined:

$$\{\, \mathbf{x} \in \mathcal{D}_{p_0} \mid \lim_{t\to\infty} \|\mathbf{\Phi}(t, \mathbf{a}) - \mathbf{\Phi}(t, \mathbf{x})\| = 0 \,\},$$

where $\mathbf{\Phi}(t, \mathbf{x})$ denotes the flow of (1) under $\mathbf{u} = \mathbf{0}$. With the phase well defined in $\mathcal{D}_{p_0}$, by changing state variables to phase coordinates, the system's asymptotic dynamic response to $\mathbf{u}$ can be characterized by a one-dimensional dynamical system:

$$\begin{aligned}
\dot{\theta} &= \frac{\partial \theta}{\partial \mathbf{x}}^\top \frac{d\mathbf{x}}{dt} \\
&= \frac{\partial \theta}{\partial \mathbf{x}}^\top \left( \mathbf{f}\left(\mathbf{x}, p_0, \mathbf{0}\right) + \frac{\partial \mathbf{f}}{\partial \mathbf{u}}\mathbf{u} + O\left(\|\mathbf{u}\|^2\right) \right) \\
&= \omega\left(p_0\right) + \mathbf{Z}(\theta, p_0)\,\mathbf{u} + O\left(\|\mathbf{u}\|^2\right) + O\left(\|\Delta\mathbf{x}\|^2\right),
\end{aligned} \tag{2}$$

where $\mathbf{Z}(\theta, p_0) = \frac{\partial \theta}{\partial \mathbf{x}}^\top \frac{\partial \mathbf{f}}{\partial \mathbf{u}}$ is often called the phase response curve (i.e. which characterizes the response to inputs), $\Delta\mathbf{x} = \mathbf{x} - \mathbf{x}^\gamma_{p_0}(\theta)$, and $^\top$ denotes the transpose. By truncating second-order terms in (2), phase reduction provides a 1-dimensional reduced system for the original $N$-dimensional system (1). However, (2) can only provide a reliable result in a close neighborhood of $\mathbf{x}^\gamma_{p_0}$, which will limit the application in the analysis of SSOs.

### B. Phase-Amplitude Reduction

It is noteworthy that the reduced-order system (2) is designed primarily to capture the timing aspects of limit cycles. A more comprehensive understanding of the system dynamics needs the integration of amplitude coordinates with phase coordinates, i.e., the phase-amplitude system which can effectively capture the dynamics governing the decay in directions transverse to a periodic orbit. In this paper, Floquet coordinates [13] are utilized to represent the effects of amplitudes. With $\Delta\mathbf{x} = \mathbf{x} - \mathbf{x}^\gamma_{p_0}(\theta)$ in mind, (1) can be approximated by the linear system $\Delta\dot{\mathbf{x}} = \mathbf{J}\mathbf{x}$ where the Jacobian $\mathbf{J}(t)$ of $\mathbf{f}$ evaluated at $\mathbf{x}^\gamma_{p_0}(\theta(t))$ is a $T(p_0)$-periodic matrix. Suppose the corresponding monodromy matrix is diagonalizable, the state can be written in the form of

$$\mathbf{x} - \mathbf{x}^\gamma_{p_0}(\theta) = \sum_{j=1}^{N-1} \psi_j \mathbf{g}_j\left(\theta, p_0\right) + \sum_{j=1}^{N-1} O\left(\psi_j^2\right) \tag{3}$$

near $\mathbf{x}^\gamma_{p_0}(\theta(t))$, where $\mathbf{g}_j\left(\theta, p_0\right) \in \mathbb{C}^N$ denotes the Floquet eigenfunction associated with the isostable coordinate $\psi_j \in \mathbb{C}$ for $j = 1, \ldots, N-1$. Note that one dimension has been absorbed due to the contribution from the Floquet eigenfunction $\mathbf{g}_N$ with Floquet multiplier $\lambda_N = 1$ by the phase coordinate, yielding $N-1$ total isostable coordinates. To linear order of accuracy, the isostable coordinates together with the phase reduction (2) yields a set of phase-amplitude reduced equations

$$\begin{aligned}
\dot{\theta} &= \omega\left(p_0\right) + \mathbf{Z}\left(\theta, p_0\right)\mathbf{u}, \\
\dot{\psi}_j &= \kappa_j\left(p_0\right) + \mathbf{I}_j\left(\theta, p_0\right)\mathbf{u}, \\
j &= 1, \ldots, \beta,
\end{aligned} \tag{4}$$

where $\mathbf{I}_j\left(\theta, p_0\right) = \frac{\partial \psi_j}{\partial \mathbf{x}}^\top \frac{\partial \mathbf{f}}{\partial \mathbf{u}}$ and all partial derivatives are evaluated at $\mathbf{x}^\gamma_{p_0}(\theta)$. The Floquet exponent $\kappa_j$ is associated with the $j^{\text{th}}$ Floquet eigenfunction $\mathbf{g}_j$. Note the dimension $\beta$ is not necessarily equal to $N-1$. Instead, $N-1-\beta$ fast decaying Floquet coordinates can be ignored and sorted by the magnitude of their associated Floquet exponents. Numerical strategies such as "adjoint method" for computing the necessary terms $\mathbf{Z}\left(\theta, p_0\right)$ and $\mathbf{I}_j\left(\theta, p_0\right)$ in both (1) and (2) are summarized in [14].

### C. Adaptive Phase-Amplitude Reduction

While (4) can provide additional amplitude information to better design control strategies, (4) together with (2) are only valid in a close neighborhood of the limit cycle $\mathbf{x}^\gamma_{p_0}(\theta)$, which means both the Floquet coordinates $\psi_j$ and input $\mathbf{u}$ should be kept small. Consequently, (2) and (4) are typically only used to analyze weakly perturbed dynamical systems.

Recently, adaptive phase-amplitude reduction [8] has been proposed to solve this issue to drive the system far from the reference limit cycle. The crucial feature of the adaptive phase-amplitude reduction strategy is that it actively updates the system parameters (and consequently the nominal limit cycle) with the explicit goal of keeping the state close to the nominal limit cycle, which means truncation errors $O\left(\psi_j^2\right)$ can be effectively kept small. Following this approach, suppose (1) has a stable limit cycle $\mathbf{x}^\gamma_p(\theta),\ \forall p \in \mathcal{B}$, where $\mathcal{B}$ is a compact set of interest including $p_0$. Immediately a family of limit cycles can be defined as $\{\, \mathbf{x}^\gamma_p(\theta) \mid p \in \mathcal{B} \,\}$ and generalized phase $\theta(\mathbf{x}, p)$ and a set of generalized Floquet coordinates $\psi_1(x, p) \ldots, \psi_\beta(x, p)$ can be defined accordingly for each $p$. Following [8], (1) can be rearranged as

$$\dot{\mathbf{x}} = \mathbf{f}(\mathbf{x}, p, \mathbf{u}) + \mathbf{u_e}(t, \mathbf{x}, p), \tag{5}$$

where

$$\mathbf{u_e}\left(t, \mathbf{x}, p\right) = \mathbf{f}\left(\mathbf{x}, p_0, \mathbf{u}\right) - \mathbf{f}(\mathbf{x}, p, \mathbf{u}).$$

979-8-3315-0995-8/25/$31.00 ©2025 IEEE

Note that (1) and (5) are identical but with different references, one can treat the vector field of (5) as $\mathbf{f}(\mathbf{x}, p, \mathbf{u})$ taking $\mathbf{u_e}$ as the equivalent input, resulting in a periodic orbit solution $\mathbf{x}_p^\gamma(\theta)$ when $\mathbf{u_e} = 0$. By appropriately choosing a time-varying parameter $p$, it is possible to limit the magnitude of the isostable coordinates, which mitigates truncation errors, resulting in a reduced-order model suitable for inputs of significant magnitude. As demonstrated in [8], the allowance for $p$ to be nonstatic, in conjunction with the phase-amplitude coordinates, leads to the following reduced-order model:

$$\begin{aligned} \dot{\theta} &= \omega(p) + \mathbf{Z}(\theta, p)\mathbf{u_e}(t, p, \mathbf{x}) + D(\theta, p)\dot{p}, \\ \dot{\psi}_j &= \kappa_j(p)\psi_j + \mathbf{I}_j(\theta, p)\mathbf{u_e}(t, p, \mathbf{x}) + Q_j(\theta, p)\dot{p}, \\ j &= 1, \ldots, \beta \\ \dot{p} &= G_p\left(p, \theta, \psi_1, \ldots, \psi_\beta\right), \end{aligned} \tag{6}$$

where

$$\begin{aligned} D(\theta, p) &\equiv \frac{\partial \theta}{\partial p} = -\frac{\partial \theta}{\partial \mathbf{x}}^\top \left.\frac{\partial \mathbf{x}^\gamma}{\partial p}\right|_{\theta,p} \in \mathbb{R}, \\ Q_j(\theta, p) &\equiv \frac{\partial \psi_j}{\partial p} = -\frac{\partial \psi_j}{\partial \mathbf{x}}^\top \left.\frac{\partial \mathbf{x}^\gamma}{\partial p}\right|_{\theta,p} \in \mathbb{C}, \\ \left.\frac{\partial \mathbf{x}^\gamma}{\partial p}\right|_{\theta,p} &\equiv \lim_{\epsilon \to 0} \frac{\left(\mathbf{x}_{p+\epsilon}^\gamma(\theta) - \mathbf{x}_p^\gamma(\theta)\right)}{\epsilon}. \end{aligned} \tag{7}$$

Note $D(\theta, p)$ and $Q_j(\theta, p)$ characterize how changes in the parameter $p$ influence $\theta$ and $\psi_j$, respectively, and provided $G_p$ can be chosen so that $\psi_j$ remains $O(\epsilon)$ for $j \leq \beta$ and that the neglected isostable coordinates have sufficiently large magnitude Floquet exponents, (5) is accurate up to $O(\epsilon)$ provided that $\mathbf{u_e}$ is an $O(1)$ term [8]. While (6) accurately captures nonlinear oscillations, the isostable coordinates $\psi_3, \ldots, \psi_\beta$ typically correspond to rapidly decaying Floquet eigenfunctions compared to those linked with $\psi_1$ and $\psi_2$. Therefore, explicitly considering these additional isostable coordinates is often unnecessary in practice. Thus, consider (6) with only the single slowest isostable coordinate:

$$\begin{aligned} \dot{\theta} &= \omega(p) + \mathbf{Z}(\theta, p)\mathbf{u_e}(t, p, \mathbf{x}) + D(\theta, p)\dot{p}, \\ \dot{\psi} &= \kappa(p)\psi + \mathbf{I}(\theta, p)\mathbf{u_e}(t, p, \mathbf{x}) + Q(\theta, p)\dot{p}, \\ \dot{p} &= G_p\left(p, \theta, \psi\right). \end{aligned} \tag{8}$$

Note that in (8) the subscript denoting the isostable coordinate index has been dropped or convenience of notation. Letting

$$G_p\left(p, \theta, \psi\right) = -\frac{\mathbf{I}(\theta, p)\mathbf{u_e}(t, p, \mathbf{x})}{Q(\theta, p)} \tag{9}$$

allows for the following simplification of (8):

$$\begin{aligned} \dot{\theta} &= \omega(p) + \mathbf{Z}(\theta, p)\mathbf{u_e}(t, p, \mathbf{x}) + D(\theta, p)\dot{p}, \\ \dot{\psi} &= \kappa(p)\psi, \\ \dot{p} &= -\frac{\mathbf{I}(\theta, p)\mathbf{u_e}(t, p, \mathbf{x})}{Q(\theta, p)}, \end{aligned} \tag{10}$$

where $\dot{\psi} = \kappa(p)\psi$ is decoupled and will converge to $\psi = 0$ as time approaches to infinity and can be ignored. The final 2-dimensional reduced-order model becomes

$$\begin{aligned} \dot{\theta} &= \omega(p) + \mathbf{Z}(\theta, p)\mathbf{u_e}(t, p, \mathbf{x}) + D(\theta, p)\dot{p}, \\ \dot{p} &= -\frac{\mathbf{I}(\theta, p)\mathbf{u_e}(t, p, \mathbf{x})}{Q(\theta, p)}. \end{aligned} \tag{11}$$

## III. Power System Model

### A. IBR Model

The model of the inverter usually includes a phase-locked loop (PLL), frequency and voltage support functions, a current limit controller, and a pulse-width modulation generator. The PLL is employed to generate frequency and angle reference signals for other components, featuring a PI controller for rotor angle control. Furthermore, Voltage and frequency support functions enhance voltage and frequency response performance. We followed the model used in [15]. Note that in this paper we mainly consider Hopf-Bifurcation-induced SSOs, so limits of controllers are disabled to avoid the influence of limit cycles induced by switching. While this model is simplified, the resulting phenomena still provide practical insights. The system model of the PLL is

$$\begin{aligned} \dot{\delta} &= \Delta\hat{\omega}, \\ \dot{\varphi} &= K_i v_q, \end{aligned} \tag{12}$$

where $\delta$ is the relative angle of the $d$-axis (PLL output angle) with respect to the terminal voltage, $\hat{\omega}$ is the output rotor angular frequency, $\Delta\hat{\omega} = \hat{\omega} - \omega_0$ is the frequency derivation with respect to the nominal frequency $\omega_0$ and $\varphi$ is the intermediate state variable involved in the PI control loop. $K_i$ and $K_p$ are gains of the PI controller in the PLL, and $v_q$ is the voltage on the $q$-axis. Note the rotor angle speed $\hat{\omega}$ and voltage on the $q$-axis $v_q$ in (12) are defined:

$$\begin{aligned} \Delta\hat{\omega} &= K_p v_q + \varphi, \\ v_q &= (i_d X + i_q R) - e_{eq}\sin\delta, \end{aligned} \tag{13}$$

where $i_d$ and $i_q$ are the output of the support function, respectively, and $e_{eq}$ is the equivalent terminal voltage magnitude. Moreover, the algebraic equations in support functions are

$$\begin{aligned} v_d &= (i_d X - i_q R) + e_{eq}\cos\delta, \\ i_d &= I_{dcon} - P_\omega \Delta\omega, \\ i_q &= P_p\left(v_d - v_{ref}\right) + \varsigma, \\ \dot{\varsigma} &= P_i\left(v_d - v_{ref}\right), \end{aligned} \tag{14}$$

where $P_p$, $P_i$, and $P_\omega$ are parameters in controllers of voltage and frequency support functions, $v_{ref}$ is the nominal value of $v_d$, and $\varsigma$ is the intermediate variable in the voltage control loop. Here the frequency droop is added on the constant set point $I_{dcon}$ in order to regulate real power. $R + \mathrm{j}X$ is the equivalent impedance between the IBR and the equivalent voltage source. A more detailed explanation of (12), (13) and (14) can be found in [15].

### B. Multi-Machine Classical Model

The $M$-machine classical model is considered in this paper, whose generators are represented by the second-order swing equation:

$$\begin{aligned} \dot{\omega}_i &= \frac{\omega_0}{2H_i}\left(P_{m,i} - P_{e,i} - D_i\frac{\omega_i - \omega_0}{\omega_0}\right), \\ \dot{\delta}_i &= \omega_i - \omega_0, \end{aligned} \tag{15}$$

where $i \in \{1, 2, \ldots, M\}$, $\delta_i$, $\omega_i$, $P_{\mathrm{m}i}$, $P_{ei}$, $H_i$ and $D_i$ respectively represent the absolute rotor angle, rotor angular speed, mechanical power, electrical power, inertia constant



979-8-3315-0995-8/25/$31.00 ©2025 IEEE

and damping constant of machine $i$, and $P_{ei} = E_i^2 g_i + \sum_{j=1,j\neq i}^{M} [a_{ij} \sin(\delta_i - \delta_j) + b_{ij} \cos(\delta_i - \delta_j)]$, where $E_i$, $g_i$, $a_{ij}$, and $b_{ij}$ represent network parameters including all loads.

## IV. Case Studies

To characterize the nonlinear SSO, the two-area system model is considered [5], and its topology is shown in Fig. 1. Generator G4 in the system is modeled as an IBR using equations (12) to (14), while generators G1 to G3 follow classical models given by (15). The specific parameters for the

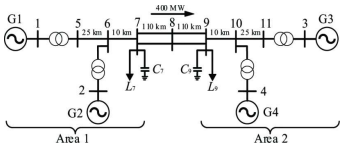


Fig. 1: Two-area system.

IBR are outlined in Table I, with the remaining parameters for the two-area system consistent with those detailed in [5]. This setting is motivated by the typical situation where the proportional gain $K_p$ is considerably smaller than the integral gain $K_i$ and is sometimes assumed to be zero in literature [15]. The eigenvalues of the linearized system at the fixed point are presented in Table II. Although the fixed point is not small-signal stable due to an unstable mode introduced by the IBR, the system dynamics converge to a limit cycle rather than diverge after a small perturbation. Oscillations are observed in all state variables, particularly, the frequency deviations of traditional generators and the current $i_q$ of the IBR participate in oscillations, the 3-second steady-state results are illustrated in Fig. 2. To characterize these oscillations, notice the damping is zero, indicating a limit cycle. Furthermore, the frequency associated with the unstable eigenpair is 5.1944 Hz, while the observed limit cycle frequency is 4.9395 Hz, indicating a nonlinear relationship between the frequency and amplitude. Typically, a well-designed power system could locally avoid the existence of a limit cycle. However, the bifurcation could happen due to the switching of some parameters or load varying, which is common in practice. Then, the stability property of the fixed point is changed, and a stable limit cycle may appear such as Fig. 2. Indeed, note this model does have a subcritical Hopf

TABLE I: Default Setting of Parameters for the IBR

| $K_i$ {(rad/s)/p.u.} | $K_p$ {(rad/s)/p.u.} | $P_\omega$ {p.u./(rad/s)} | $P_i$ (p.u./p.u.) | $P_p$ (p.u./p.u.) |
|---|---|---|---|---|
| 1400 | 1.9 | 0.0027 | 200 | 0 |

TABLE II: Eigenvalues and Corresponding Modes

| Eigenvalue | Mode Type | Frequency (Hz) |
|---|---|---|
| $0.1931 + 32.6373\text{i}$<br>$0.1931 - 32.6373\text{i}$ | Unstable | 5.1947 |
| $-0.1933 + 7.3215\text{i}$<br>$-0.1933 - 7.3215\text{i}$ | Stable | 1.1482 |
| $-0.1865 + 3.9576\text{i}$<br>$-0.1865 - 3.9576\text{i}$ | Stable | 0.6299 |
| $-0.3881$ | Non oscillation | 0 |
| $-11.9342$ | Non oscillation | 0 |

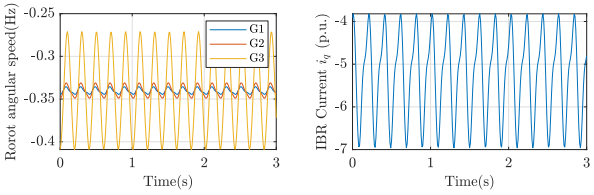


(a) Frequency derivations (b) Current of the IBR in $q$-axis

Fig. 2: Nonlinear SSOs involving the IBR

bifurcation [6] at $K_p = 2.0209$ (or $P_i = 186.4$) when all other parameters are held constant. The accurate 2-dimensional reduced order nonlinear model (11) can be employed for this specific bifurcation. The nonstatic parameter $p$ in (11) can be selected as either $K_p$ or $P_i$. For the sake of generality, both are considered, resulting in two reduced-order models. The first (resp., second) model has 2 variables: $p \in [1.2, 2.02]$ (resp., $p \in [186.4, 208]$) parameterizes the set of limit cycles that result when taking different constant values of $K_p$ (resp., $P_i$); $\theta$ is the phase along a given limit cycle. Intuitively, moving $p$ closer to 2.02 (resp., 186.4) moves the system close to the Hopf bifurcation and reduces the amplitude of oscillations. By setting a series of different initial conditions for (11), the relationship between the amplitude of the SSO of IBR's frequency deviation $\Delta\hat{\omega}$ and its natural frequency (denoted as $\omega(p)$ in (11)) is effectively characterized, and the resulting Frequency-Amplitude (F-A) curve is illustrated in Fig. 3. It can be concluded that the natural frequency of the SSO increases as its amplitude decreases until the frequency approaches 5.1947 Hz, indicating the occurrence of the bifurcation. These findings explore the nonlinearity of the SSO, and both models accurately capture its dynamics, demonstrating accuracy even near the bifurcation point. The SSO is recreated using the phasor model [15], capable of capturing oscillatory dynamics induced by the control parameters of IBRs. Note that this case is not isolated and can be replicated in more complex systems. For instance, a 5.7-Hz nonlinear SSO event was simulated using NREL's ParaEMT platform on the WECC EMT model, illustrating the presence of SSOs in larger, more detailed systems [16].

To further validate the accuracy of proposed models, dynamic responses to the step change of parameters are first considered, setting $P_\omega$ to $8\times10^{-3}$ at $t = 0$ s and then adjusting it to $3.8 \times 10^{-4}$ at $t = 2.5$ s. Corresponding 5s simulation results of system responses are shown in Fig 4. In the first (resp., second) model, $p$ increases (resp., decreases), bringing the system closer to the Hopf bifurcation until $t = 2.5$ s and then decreases (resp., increases), moving away from the bifurcation. While the behavior of the reduced-order and full-order models closely align, perfect matching of model dynamics is generally not expected due to the truncation of lower amplitude modes $\psi$ in both reduced-order systems. Moreover, an input $\mathbf{u} := [0\ 0\ 0\ 0\ 0\ 0\ 0\ -k\Delta\hat{\omega}\ 0]^\top$ in (1), (i.e., changing $\dot{\varphi} = K_i V_q - k\Delta\hat{\omega}$) is designed to verify responses of reduced-order models, here $k = 0.2$. 5s simulation results are shown in Fig. 5. The additional input $\mathbf{u}$ can drive the system back to the stable operation indicated by the increasing natural frequency $\omega(p)$, and both reduced-order 2-dimensional models

979-8-3315-0995-8/25/$31.00 ©2025 IEEE

can accurately capture the dynamics along simulations before bifurcation happens when $\omega(p)$ approaches 5.19 Hz. Note that the relative errors in Fig 4d and Fig. 5d are due to the accumulation of errors associated with the oscillation phase $\theta$. It is crucial to emphasize that both the frequency and amplitude of the reduced-order models exhibit a close alignment with the full-order models throughout the entire simulation, which can be observed from Fig 4b and Fig. 5b. The consistency in matching frequency and amplitude demonstrates the reliability and accuracy of the reduced-order models in capturing the essential dynamics, providing a comprehensive understanding of the system's behavior.

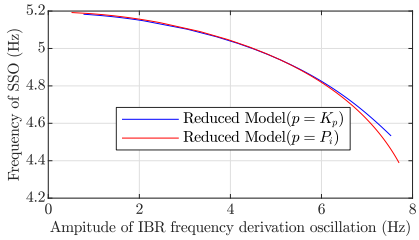


Fig. 3: Frquency-Amplitude characterization of the SSO

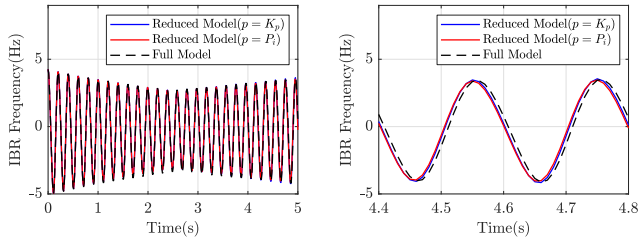


(a) Frequency derivations (b) Zoomed view of (a)

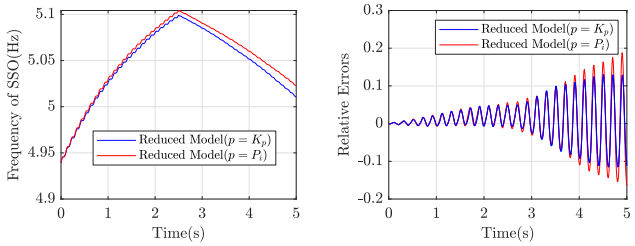


(c) Natural frequency of the SSO (d) Relative errors

Fig. 4: System response to the changing of $K_\omega$

## V. Conclusion and Future Work

In this paper, a nonlinear SSO has been studied and characterized, in particular, a reduced-order model is introduced which leverages recently developed adaptive phase-amplitude reduction techniques. By parameterizing a family of limit cycles associated with a particular parameter $p$, a 2-dimensional reduced-order model of the form (11). The result shows it accurately replicates large amplitude nonlinear oscillation dynamics, in response to the step change of parameters and external forcing. In future work, the reduced-order model will be applied to stability analysis and control of such IBR-induced nonlinear SSOs.

## References


[1] L. Fan, Z. Miao, S. Shah, Y. Cheng, J. Rose, S.-H. Huang, B. Pal, X. Xie, N. Modi, S. Wang, and S. Zhu, "Real-world 20-hz ibr subsynchronous oscillations: Signatures and mechanism analysis," *IEEE Transactions on Energy Conversion*, vol. 37, no. 4, pp. 2863–2873, 2022.


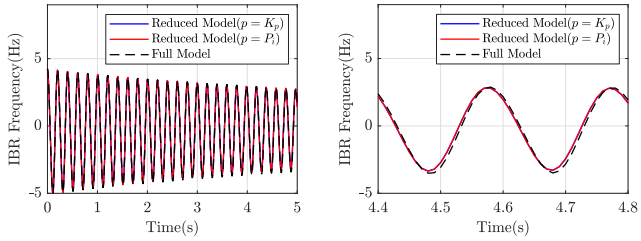


(a) Frequency derivations (b) Zoomed view of (a)

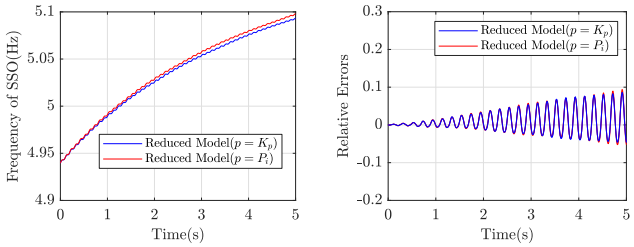


(c) Natural frequency of the SSO (d) Relative errors

Fig. 5: System response when adding $\mathbf{u}$


[2] J. Shair, X. Xie, J. Yang, J. Li, and H. Li, "Adaptive damping control of subsynchronous oscillation in dfig-based wind farms connected to series-compensated network," *IEEE Transactions on Power Delivery*, vol. 37, no. 2, pp. 1036–1049, 2022.

[3] I. A. Hiskens and P. B. Reddy, "Switching-induced stable limit cycles," *Nonlinear Dynamics*, vol. 50, pp. 575–585, 2007.

[4] M. L. Sosa-Ríos, L. F. C. Alberto, R. A. Ramos, and F. Bizzarri, "Method for characterization of limit cycles in power systems," in *2023 IEEE Power & Energy Society General Meeting (PESGM)*, 2023, pp. 1–5.

[5] P. Kundur, *Power System Stability and Control*, ser. EPRI power system engineering series. McGraw-Hill Education, 1994.

[6] G. B. Ermentrout and D. H. Terman, *Neural Oscillators: Weak Coupling*. New York, NY: Springer New York, 2010, pp. 171–240.

[7] D. Wilson, "Optimal control of oscillation timing and entrainment using large magnitude inputs: An adaptive phase-amplitude-coordinate-based approach," *SIAM Journal on Applied Dynamical Systems*, vol. 20, no. 4, pp. 1814–1843, 2021.

[8] ——, "An adaptive phase-amplitude reduction framework without $\mathcal{O}(\epsilon)$ constraints on inputs," *SIAM Journal on Applied Dynamical Systems*, vol. 21, no. 1, pp. 204–230, 2022.

[9] D. Wilson and K. Sun, "Reduced order characterization of nonlinear oscillations using an adaptive phase-amplitude coordinate framework," *SIAM Journal on Applied Dynamical Systems*, In Press.

[10] G. B. Ermentrout and D. H. Terman, *Mathematical Foundations of Neuroscience*. New York: Springer, 2010, vol. 35.

[11] D. Wilson and J. Moehlis, "Isostable reduction of periodic orbits," *Phys. Rev. E*, vol. 94, p. 052213, Nov 2016.

[12] A. Mauroy, I. Mezić, and J. Moehlis, "Isostables, isochrons, and koopman spectrum for the action–angle representation of stable fixed point dynamics," *Physica D: Nonlinear Phenomena*, vol. 261, pp. 19–30, 2013.

[13] D. Jordan and P. Smith, *Nonlinear Ordinary Differential Equations:An Introduction for Scientists and Engineers: An Introduction for Scientists and Engineers*, ser. Oxford Texts in Applied and Engineering Mathematics. OUP Oxford, 2007.

[14] B. Monga, D. Wilson, T. Matchen, and J. Moehlis, "Phase reduction and phase-based optimal control for biological systems: a tutorial," *Biological Cybernetics*, vol. 113, no. 1-2, pp. 11–46, 2019.

[15] Z. Zhou, W. Wang, D. Ramasubramanian, E. Farantatos, and G. M. Huang, "Small signal stability of phase locked loop based current-controlled inverter in 100% inverter-based system," *IEEE Transactions on Sustainable Energy*, vol. 14, no. 3, pp. 1612–1623, 2023.

[16] M. Xiong, B. Wang, D. Vaidhynathan, J. Maack, M. Reynolds, A. Hoke, K. Sun, and J. Tan, "Paraemt: An open source, parallelizable, and hpc-compatible emt simulator for large-scale ibr-rich power grids," *IEEE Transactions on Power Delivery*, pp. 1–11, 2023.



979-8-3315-0995-8/25/$31.00 ©2025 IEEE